

# The local luminosity function of QSOs and Seyfert 1 nuclei<sup>\*</sup>

T. Köhler, D. Groote, D. Reimers, and L. Wisotzki

Hamburger Sternwarte, Gojenbergsweg 112, D-21029 Hamburg, Germany

Received ; accepted

**Abstract.** We present the analysis of a new flux-limited sample of bright quasars and Seyfert 1 galaxies in an effective area of  $611 \text{ deg}^2$ , drawn from the Hamburg/ESO survey. We confirm recent claims that bright quasars have a higher surface density than previously thought. Special care was taken to avoid morphological and photometric biases against low-redshift quasars, and about 50% of the sample objects are at  $z < 0.3$ , spanning a range of  $\Delta M \simeq 8$  in absolute magnitudes. While our derived space densities for low-luminosity Seyfert 1 nuclei are consistent with those found in the literature, we find that luminous QSOs,  $M_B < -24$ , are much more numerous in the local universe than previous surveys indicated. The optical luminosity functions of Seyfert 1 nuclei and QSOs join smoothly, and if the host galaxy contributions are taken into account, a single power-law of slope  $\alpha = -2.2$  describes the combined local luminosity function adequately, over the full range in absolute magnitude. Comparing our data with published results at higher redshifts, we can rule out pure luminosity evolution as an acceptable parametrisation; the luminosity function of quasars changes shape and slope with  $z$ , in the sense that the most luminous quasars show the weakest evolution.

**Key words:** Galaxies: luminosity function – Quasars: general – Galaxies: Seyfert

## 1. Introduction

The average luminosities of quasars, and possibly many other properties, depend strongly on cosmological epoch. Shape, normalisation, and evolution of the quasar luminosity function (QLF) are among the most basic descriptions of the quasar population. A good knowledge of the local ( $z \approx 0$ ) QLF is essential for at least two purposes:

*Send offprint requests to:* L. Wisotzki,  
email: lwisotzki@hs.uni-hamburg.de

<sup>\*</sup> Based on observations made at the European Southern Observatory, La Silla, Chile

first, to serve as zero-point for quasar evolution studies; second, to provide a reference distribution law for unbiased subsamples constructed for statistical investigations (e.g., for spectral properties, host galaxies, etc).

Unfortunately, current determinations of the QLF are limited mainly to  $z \gtrsim 0.3$ , for the simple reason of lacking appropriate survey data. Most optical QSO surveys discriminate against objects with extended morphology, causing severe incompleteness (and bias) at low redshifts. At the low-luminosity end of the QSO–Seyfert family, dedicated galaxy surveys have prompted investigations of the Seyfert 1 luminosity function (e.g., Cheng et al. 1985; Huchra & Burg 1992). However, these surveys are necessarily incomplete at *high* nuclear luminosities, where the active nuclei outshine the surrounding hosts, and the objects are not selected as galaxies anymore.

In 1990 we started the ‘Hamburg/ESO survey’ (HES), a new wide-angle survey for bright QSOs and Seyferts, designed to avoid the above selection biases as far as possible. A detailed description of the HES was given by Wisotzki et al. (1996; hereafter Paper I), and a first list of 160 newly discovered QSOs was published by Reimers et al. (1996; Paper II). Basically, QSO candidates are selected by automated procedures from digitised objective-prism plates taken with the ESO Schmidt telescope, with subsequent slit spectroscopy of all candidates above the magnitude limit of typically  $B_{\text{lim}} \simeq 17.0\text{--}17.5$ , over an area of  $\sim 5000 \text{ deg}^2$  at high galactic latitude. To prevent morphological bias against sources with resolved structure, such as Seyferts or gravitational lenses, objects with non-stellar appearance are *not* excluded from the candidate lists. Among other goals, we aim to construct a large, optically flux-limited sample of low-redshift ‘Type 1 AGN’, including QSO/Seyfert borderline objects.

In this paper we publish the results of an analysis of a first part of the HES, based on 33 Schmidt fields, with an effective area of  $611 \text{ deg}^2$ . We present the first direct determination of the local quasar luminosity function from a single optical survey, and discuss some implications of our results. A comprehensive description of the analysis has been given by Köhler (?). We adopt a cosmological model with  $H_0 = 50 \text{ km s}^{-1} \text{ Mpc}^{-1}$ ,  $q_0 = 0.5$ , and  $\Lambda = 0$ .

**Table 1.** Properties of surveyed fields. Field designations are given as standard ESO/SERC field numbers.  $N_H$  is the column density of Galactic neutral hydrogen in the field centre, in  $10^{20} \text{ cm}^{-2}$ .  $A_B$  is the corresponding extinction in the  $B$  band.  $\Omega_{\text{eff}}$  is the effective survey area for the field, in  $\text{deg}^2$ .

Field	$B_{\text{lim}}$	$N_H$	$A_B$	$\Omega_{\text{eff}}$
501	17.38	5.5	0.39	16.38
503	17.25	4.8	0.34	17.75
505	16.95	7.4	0.53	17.05
506	17.66	7.5	0.54	17.17
507	17.11	7.2	0.51	17.10
509	16.95	5.3	0.38	17.04
568	16.95	5.8	0.41	18.20
570	16.78	4.2	0.30	18.92
578	16.64	6.2	0.44	17.59
637	16.90	5.5	0.39	17.94
638	16.95	7.5	0.53	16.14
639	17.47	5.1	0.36	19.35
640	17.50	4.9	0.35	16.23
643	17.41	4.4	0.31	21.47
644	17.31	3.9	0.28	18.46
645	17.42	3.8	0.27	20.72
646	17.23	4.0	0.28	17.68
647	17.46	5.2	0.37	20.02
648	17.15	6.2	0.44	17.95
649	17.05	7.3	0.52	16.68
650	17.15	7.4	0.53	11.86
708	17.21	4.2	0.30	20.12
709	17.46	5.7	0.41	20.07
710	17.62	4.8	0.34	22.91
711	17.11	3.5	0.25	19.74
715	17.35	4.1	0.29	21.52
716	16.78	3.2	0.23	18.71
717	17.14	2.5	0.17	17.64
718	17.35	3.4	0.24	20.39
719	17.25	2.5	0.18	20.20
720	17.30	3.7	0.26	19.85
721	17.14	3.6	0.25	19.39
722	16.86	5.8	0.41	18.95

## 2. The quasar sample

### 2.1. Survey area

The investigated area was defined by 33 ESO Schmidt fields located in the region  $-28^\circ < \delta < -7^\circ$  and  $9^{\text{h}} 40^{\text{m}} < \alpha < 14^{\text{h}} 40^{\text{m}}$ , thus all in the North Galactic hemisphere. A list of the survey fields and their properties is given in Table 1.

In each field, one direct plate from the ESO (B) atlas, and one HES spectral (objective prism) plate were available. The formal total area subtended by 33 ESO plates is  $\sim 25 \text{ deg}^2 \times 33 = 825 \text{ deg}^2$ . Losses of usable area occurred because (1) plates overlapped in adjacent fields, especially if not precisely centred; (2) occasionally direct and spectral plates were positionally mismatched, and only the common area could be used; (3) most important, overlapping spectra (and to a lesser degree, direct images) ren-

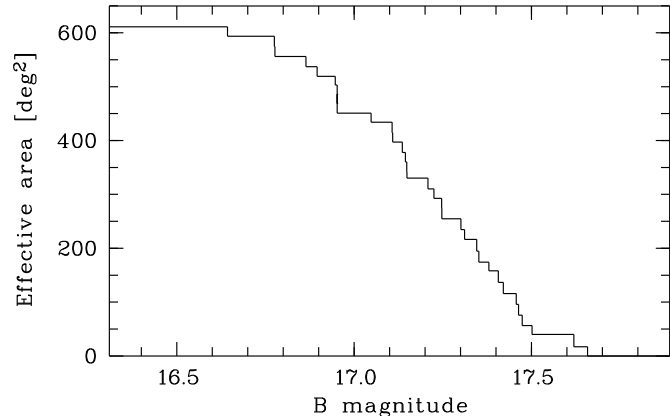


**Fig. 1.** Effective area of the surveyed region as a function of  $B$  magnitude (without correction for Galactic extinction).

dered a certain percentage of spectra unprocessable. These losses have been quantified and incorporated into ‘effective areas’  $\Omega_{\text{eff}}$  for each field, given in Table 1. Because of the field-to-field variations in limiting magnitude, the total effective survey area is a function of apparent magnitude, as plotted in Fig. 1. The maximum area is  $611 \text{ deg}^2$  for  $B < 16.64$  and decreases gradually to zero for sources fainter than  $B = 17.66$ .

While many quasar surveys were carried out at very high Galactic latitudes where foreground extinction corrections are small (although systematically non-zero), this is not the case for our present set of fields. We have used the data from Stark et al. (1992) to obtain the neutral hydrogen column density in the centre of each field, and converted this into a  $B$  band extinction using the formula  $A_B = 4.2 \times N_H / 59$  where  $N_H$  is given in units of  $10^{20} \text{ cm}^{-2}$  (cf. Spitzer 1978); Table 1 lists  $N_H$  and  $A_B$  for each field. The average extinction is 0.36 mag.

### 2.2. Sample selection

The limiting brightness of QSO candidates during the automated selection procedure was initially defined by a minimum S/N ratio of  $\sim 3$  in the digital spectra. We later found, as expected (cf. Paper I), that close to the selection limit the object lists became incomplete. Several experiments showed that systematic incompleteness occurred only for the faintest spectra, and that the effect disappeared for a limiting  $S/N \geq 5$ . We translated this S/N cutoff into a magnitude limit on the direct plate, using the calibration of photographic magnitudes described below. For the 33 fields, the values for  $B_{\text{lim}}$  range between 17.66 and 16.64, depending largely on the quality of the spectral plates.

Altogether, 115 QSOs and Seyfert 1 galaxies were detected by the HES selection criteria in these fields (primarily different measures of UV excess; cf. Paper I) that were either confirmed by our own follow-up spectroscopy

**Table 2.** The flux-limited sample of QSOs with  $z > 0.07$ . The entries in column  $B$  marked by colons are photographic, all other magnitudes are CCD measurements corrected to the zero-points of the photographic plates. Column  $B_0$  lists the extinction-corrected magnitudes.

Name	$z$	$B$	Field	$B_0$	$M_B$
HE 0952–1552	0.108	16.56	637	16.17	–22.87
HE 1006–1211	0.693	16.37	709	15.96	–27.03
HE 1007–1405	0.583	16.05	637	15.66	–26.94
HE 1012–1637	0.433	16.22	638	15.69	–26.25
HE 1015–1618	0.247	15.91:	638	15.38	–25.40
HE 1019–1413	0.077	16.75	638	16.22	–22.09
PKS 1020–103	0.197	17.39	710	17.05	–23.26
HE 1021–0738	1.800	17.47	710	17.12	–28.00
PKS 1022–102	2.000	17.58	710	17.24	–28.14
HE 1025–1915	0.323	16.91	568	16.50	–24.84
HE 1029–1401	0.086	14.07	638	13.54	–25.01
HE 1031–1457	0.652	17.39	639	17.03	–25.83
HE 1041–1447	1.569	17.26:	639	16.90	–27.91
HE 1043–1443	0.599	17.06	639	16.70	–25.96
HE 1045–2322	0.407	16.65	501	16.26	–25.55
PKS 1048–090	0.345	16.51	711	16.27	–25.21
HE 1104–1805	2.319	16.30	570	16.00	–29.62
HE 1109–1255	0.596	17.19	640	16.84	–25.80
HE 1110–1910	0.111	16.77	570	16.47	–22.63
HE 1115–1735	0.217	16.25	570	15.95	–24.56
HE 1120–2713	0.389	16.94	503	16.60	–25.12
HE 1159–1338	0.506	16.68	643	16.36	–25.91
HE 1200–1234	0.553	17.22	643	16.91	–25.56
HE 1201–2409	0.137	16.74	505	16.21	–23.33
HE 1211–1322	1.125	16.15	644	15.87	–28.25
HE 1223–1543	1.735	17.14	644	16.86	–28.17
HE 1228–1637	0.102	16.78	644	16.50	–22.43
HE 1233–2313	0.238	17.06	506	16.52	–24.18
HE 1237–2252	0.096	17.29	506	16.75	–22.05
HE 1239–2426	0.082	16.73	507	16.22	–22.25
HE 1254–0934	0.139	15.72	718	15.48	–24.11
HE 1255–2231	0.492	17.02	507	16.51	–25.71
HE 1258–0823	1.153	16.44	718	16.20	–27.97
HE 1258–1627	1.709	17.22	646	16.94	–28.06
PKS 1302–102	0.278	15.15	718	14.91	–26.12
HE 1304–1157	0.294	17.14	718	16.90	–24.25
HE 1312–1200	0.327	16.07	719	15.89	–25.48
HE 1315–1028	0.099	16.75	719	16.57	–22.28
Q 1316–0734	0.538	16.70	719	16.52	–25.89
HE 1335–0847	0.080	16.80	720	16.54	–21.86
HE 1341–1020	2.134	17.28	720	17.02	–28.48
HE 1345–0756	0.777	17.13	720	16.87	–26.40
HE 1358–1157	0.408	16.64:	721	16.39	–25.43
HE 1403–1137	0.589	16.86	721	16.61	–26.01
HE 1405–1545	0.194	16.51	649	15.99	–24.29
HE 1405–1722	0.661	15.85	649	15.33	–27.55
PG 1416–1256	0.129	16.88	650	16.35	–23.07
HE 1419–1048	0.265	16.77	722	16.36	–24.58

(Paper II), or previously catalogued as QSO or Seyfert 1 in the compilation of Véron-Cetty & Véron (1993). Note that in this paper we deliberately ignore the traditional

subdivision Seyferts vs. ‘real’ QSOs based on some arbitrary luminosity threshold. A lower redshift limit of 0.07 was applied to avoid possible incompleteness due to host galaxy contamination (but see the  $z < 0.07$  Seyfert sample below). Several of the lowest redshift objects would nevertheless be called Seyferts by many others.

There remained 48 QSOs with  $z > 0.07$  located within the effective survey area and above the completeness limiting magnitude. These form the flux-limited sample listed in Table 2. A comparison with the Véron-Cetty & Véron (1993) catalogue revealed no additional QSOs that should have been included in the flux-limited sample. This test for ‘completeness’ is, however, not very strong, as few other surveys have covered this region of the sky, and  $\sim 90\%$  of the sample objects are new discoveries made by the HES.

### 2.3. Photometry

Obtaining consistent and unbiased photometry of low-redshift quasars with detectable host galaxies is not trivial. During the survey phase, normally only photographic data, in our case from the digitised direct  $B$  plates, are available. These plates usually reach much fainter magnitudes than objective-prism plates, but they also saturate earlier, especially if not the original plates but glass copies are used (as was the case for several of our fields). The conventionally employed isophotal or large aperture magnitudes, although well suited for point sources, tend to give much larger total luminosities for QSOs with detectable hosts than desired for an investigation of the *nuclear* luminosity function. Additional complications can result from non-linear filtering effects inherent in the digitisation procedure.

For the present sample we have developed a two-step procedure to obtain unbiased and survey-consistent magnitudes. The photographic plates were calibrated by CCD sequences obtained with the ESO 90 cm telescope in 1993 and 1994. These sequences will be published in a separate paper. The sample selection was based on simulated diaphragm photometry with an aperture of the size of the seeing disk. For point sources, an accurate calibration relation with very little intrinsic scatter,  $\sim 0.15$  mag, could be derived from the CCD sequences (which contained only stars). These small-aperture magnitudes correlated also well with the corresponding S/N ratios of the digital spectra, important for an accurate definition of limiting magnitudes.

In a second step, we obtained CCD photometry for most of the sample QSOs. Exposures in the  $B$  band were available from the mandatory acquisition images at the ESO 3.6 m and 2.2 m telescopes (cf. Paper II). After standard reduction and colour term corrections, the photometric zero points of these images were shifted to the system of the corresponding photographic plate by using surrounding unsaturated field stars as references. The resulting corrected CCD magnitudes, again measured in an aper-

**Table 3.** Seyfert 1 galaxies with  $z < 0.07$ . The CCD magnitudes are for the small aperture (see text). Absolute magnitudes are given as observed ( $M_{B,\text{obs}}$ ), and with host galaxy contribution  $M_{\text{gal}}$  subtracted ( $M_{\text{nuc}}$ ).

Name	$z$	$B$	Field	$B_0$	$z_{\text{max}}$	$V_e/V_a$	$M_{B,\text{obs}}$	$M_{\text{gal}}$	$M_{\text{nuc}}$
HE 1043–1346	0.0669	16.83	639	16.47	0.0692	0.902	−21.55	−21.06	−20.44
HE 1248–1357	0.0144	15.28	645	15.01	0.0152	0.855	−19.67	−19.39	−18.06
IRAS 1249–13	0.0129	14.91	645	14.64	0.0254	0.132	−19.80	−19.10	−18.99
R 12.01	0.0463	15.50	646	15.21	0.0700	0.289	−22.00	−20.90	−21.52
PG 1310–1051	0.0337	15.64	719	15.46	0.0544	0.238	−21.07	−19.54	−20.77
HE 1330–1013	0.0221	15.82	719	15.65	0.0293	0.428	−19.96	−18.96	−19.41
R 14.01	0.0408	14.68	648	14.24	0.0700	0.196	−22.70	−20.72	−22.51

ture of diameter approximately equal to that of the seeing disk, should be much more accurate than the photographic data, at least for extended objects, while magnitudes of point sources should be more or less unchanged. We tested this assertion by comparing photographic and zero-point corrected CCD photometry of the  $z > 0.3$  QSOs (which should be true point sources) and found a mean difference of only 0.01 mag. For the further analysis we used the zero-point corrected  $B$  band CCD magnitudes. For three objects no CCD data were available, and for those we substituted the photographic measurements (cf. Table 2).

#### 2.4. The additional Seyfert sample

To obtain further insight into the continuity of properties between high-luminosity QSOs and low-luminosity Seyfert nuclei, we conducted a dedicated subsurvey for Seyfert galaxies, targeting both type 1 and type 2 objects. The criteria were different from those used in the main survey, adapted to discriminate between active and inactive galaxies rather than between stars and QSOs. More details about this subsurvey will be given in a later paper (Köhler et al., in prep.) where we shall also present our results concerning Seyfert 2 galaxies, which we do not consider here.

We found 7 Seyfert 1 galaxies with  $0.01 < z < 0.07$ , listed in Table 3. The redshifts were remeasured in new spectra obtained with the ESO 1.52 m telescope, and corrected for heliocentric motion. Not all the fields from Table 1 were involved in this subsurvey, and the effective area was only 477 deg<sup>2</sup> (but see Sect. 4.2 for the computation of space densities).

For these sources, proper photometry is at least as important as for QSOs. The photometric systems of many earlier investigations of the luminosity function of Seyferts suffer from two severe drawbacks: (i) They were often based on heterogeneous collections of published (aperture) photometry, generally inconsistent with the magnitudes used for defining the survey flux limits. (ii) The contributions of host galaxies were either not corrected for at all, or some assumptions about universal intrinsic proper-

ties of hosts and nuclei had to be made, such as colours (Sandage 1973) or host luminosities (Cheng et al. 1985).

On the assumption that Seyfert 1 galaxies are the low-luminosity equivalent of quasars, the quantity of interest is the *nuclear* brightness, with the host galaxy contribution removed. Although our small-aperture magnitudes were already much less affected by galaxy contamination than large-aperture or total brightness measurements, a major contribution could still be expected especially for the lowest nuclear luminosities. We therefore estimated these corrections individually, based on  $B$  and  $V$  images of the seven sample objects taken with the ESO 90 cm telescope. We first constructed empirical two-dimensional point-spread functions from nearby stars. These were then subtracted from the Seyfert images, scaled by a factor chosen such that the residual galaxy surface brightness distribution did not decrease inwards. The resulting host galaxy brightness was finally integrated over the aperture and subtracted from the total aperture flux. As can be seen in Table 3, the corrections were not negligible, and – expectedly – largest for the lowest redshift sources.

### 3. The surface density of bright QSOs

An important diagnostic tool for QSO samples is the empirical relation between source fluxes and the number of sources per unit solid angle. Once the field properties and the sample photometry are complete, the cumulative surface density of QSOs brighter than magnitude  $B$ ,  $N(< B)$ , can be easily computed from summing over  $1/\Omega_{\text{eff}}$  for all relevant sample objects. From our QSO sample with  $z < 2.2$  (47 objects) we have derived the  $N(< B)$  relation shown as thick line in Fig. 2. Note that the abscissa values in this diagram are extinction-corrected magnitudes. The bright end of the curve is dominated by the extremely luminous source HE 1029–1401, but the main part can be well approximated by a simple power law of slope  $\beta = 0.67 \pm 0.04$  ( $\log N = \beta B + \text{const}$ ). If only the 33 sources with  $z > 0.2$  are considered, excluding thereby all QSO/Seyfert borderline cases (thin line in Fig. 2), the normalisation drops slightly but the slope is essentially unchanged with  $\beta = 0.69 \pm 0.05$ . For those readers who prefer differential surface densities, we have computed the

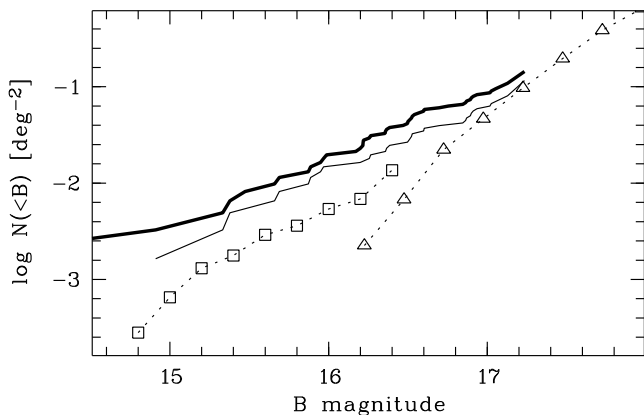


**Fig. 2.** Cumulative surface densities of bright QSOs with  $z < 2.2$ . Thick line: this work, for  $z > 0.07$ , thin line: the same for  $z > 0.2$ . Open squares show the relation from Schmidt & Green (1983), modified for  $z > 0.07$  (see text). Triangles give the LBQS (Hewett et al. 1995) relation, valid for  $z > 0.2$ .

**Table 4.** Differential surface density  $A(B)$  of 33 HES QSOs with redshifts  $0.2 < z < 2.2$ , expressed as number of QSOs per  $\text{deg}^2$  per unit magnitude interval.  $n$  gives the actually observed number per half magnitude bin ( $B \pm 0.25$ ).

$B$	$n$	$A(B)$	$\sigma_A$
15.0	1	0.003	0.003
15.5	4	0.013	0.007
16.0	5	0.016	0.008
16.5	12	0.046	0.014
17.0	11	0.15	0.08

figures in half magnitude bins between  $B = 14.75$  and  $B = 17.25$  (Table 4). The counts were multiplied by a factor of 2 to formally express number counts per unit magnitude intervals.

Comparison relations from other surveys are numerous for fainter magnitudes, but rare for  $B \lesssim 16.5$ . The Palomar Bright Quasar Survey (BQS; Schmidt & Green 1983, hereafter quoted as SG83) provides the only available optically selected QSO sample with a well-defined flux limit subtending over a similar region in the Hubble diagram. SG83 listed differential surface densities computed from the full set of 114 QSOs with  $z < 2.2$  found over an area of  $10\,714 \text{ deg}^2$ . To make their numbers comparable to ours, we recomputed the BQS surface densities by removing all  $z < 0.07$  entries from their sample, and converted the result into a cumulative relation. This relation is shown in Fig. 2 by the open squares. A large discrepancy at all magnitudes is apparent. At  $B = 16$ , the surface density found in the HES is high by a factor of 3.6 compared to the BQS, certainly more than can be permitted by statistical fluctuations.

A similar result was already reported by Goldschmidt et al. (1992) from an analysis of the Edinburgh sur-

vey, who found 5 QSOs above the BQS flux limit in an area of  $330 \text{ deg}^2$  (non-overlapping with the present HES area) while the BQS contained only one. Their estimate of  $N(B < 16.5) = 0.024 \text{ deg}^{-2}$  for  $0.3 < z < 2.2$  is completely consistent with our corresponding value of  $0.021 \pm 0.05$ . Furthermore, Goldschmidt et al. found a zero-point offset of 0.28 mag between the BQS photographic magnitudes and theirs, in the sense that the Palomar measurements were systematically *too bright*, thus increasing rather than relaxing the discrepancy.

It should be noted that neither SG83 nor Goldschmidt et al. corrected their magnitudes for Galactic extinction, whereas we have done so. However, our survey area is *predominantly* located in regions of rather high  $A_B$ , while SG83 estimated that the extinction for most BQS quasars were ‘not much more than 0.1 mag’; this even might be, at least partly, compensated by the above mentioned zero-point offset. Because of these uncertainties we have not attempted to correct the BQS results for extinction. One can estimate globally that an average  $A_B(\text{BQS})$  of 0.61 mag would be necessary to bring BQS and HES surface densities to a match – a totally unrealistic value.

At fainter magnitudes the agreement of HES number counts with those of other surveys is excellent. As an example, we have plotted the values from the LBQS (Hewett et al. 1995) into Fig. 2, with the abscissa shifted by +0.1 mag to transform their  $B_J$  photometric system approximately into  $B$  magnitudes. While the counts in the brightest bins are again lower than ours, this can be understood as a result of poor statistics in the LBQS for  $B \lesssim 16.5$ , possibly arising from saturation effects. Around  $B \simeq 17$ , HES and LBQS surface densities join smoothly, without any detectable significant offset. Similarly good agreement is reached with other surveys, cf. the recent compilation by Cristiani et al. 1995. We are thus confident that the photometric scale used in the present investigation is essentially unbiased and adequate for luminosity function work.

## 4. Luminosity functions

### 4.1. The luminosity function of low-redshift QSOs

For all objects in Table 2, we first estimated absolute magnitudes for the rest-frame  $B$  band by computing their luminosity distances in an expanding Friedmann universe with the formula of Terrell (1977), and applying  $K$  corrections taken from Cristiani & Vio (1990). As low-redshift subsample we selected the 20 QSOs with  $z < 0.3$ . Space densities were derived using the generalised  $1/V_{\text{max}}$  estimator (Felten 1976; Avni & Bahcall 1980), thus incorporating the full information about field-dependent flux limits, including fields with zero detections (the ‘coherent’ analysis in the terminology of Avni & Bahcall).

The resulting cumulative luminosity function is shown in Fig. 3. Locations of individual objects are indicated by

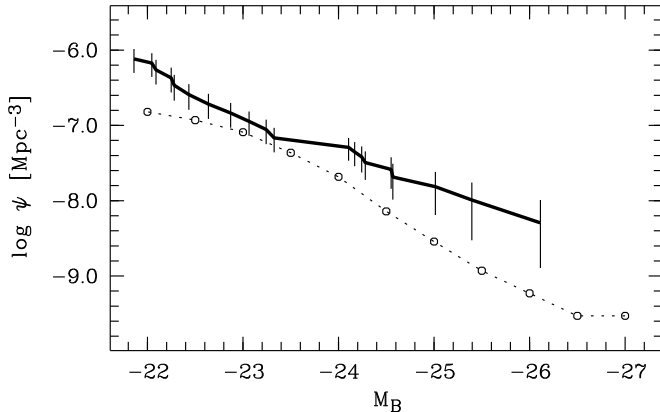


**Fig. 3.** Cumulative luminosity function of QSOs with  $0.07 < z < 0.3$  (thick line). For comparison: Cumulative luminosity function of BQS quasars with  $0.07 < z < 0.3$ , constructed as described in the text (dotted line and small symbols).

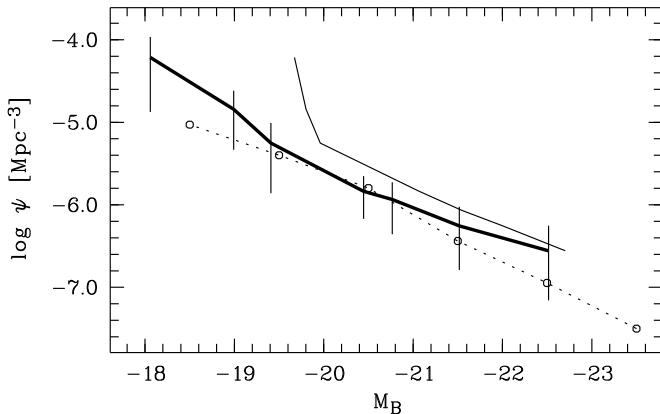


**Fig. 4.** Cumulative luminosity function of the additional Seyfert 1 sample ( $z < 0.07$ ). Thick line: LF for nuclear magnitudes corrected for the host galaxy contributions; thin line: uncorrected LF. For comparison: Seyfert 1 nuclear luminosity function of Cheng et al. (1985; dotted line and small symbols)

the error bars. We have chosen the cumulative representation  $\psi(< M_B)$  as it allows one to avoid binning (particularly problematic for smaller samples) and to make the contribution of each object in the sample apparent. The errors were estimated from Poisson statistics in the sample, combined with the uncertainties in volume determination resulting from the photometric errors.

Restricting the HES luminosity function to  $z < 0.2$  (14 objects) results in slightly larger error bars, but the space densities change only insignificantly, by less than 0.05 dex, and, overplotted in Fig. 3, could not even be distinguished from the  $z < 0.3$  relation. We thus feel justified to neglect differential evolution within our redshift shell; we shall further investigate and qualify this assumption below.

Up to now, the BQS provides the only comparison sample in the region  $M_B < -23$  and  $z < 0.3$ , containing 45 objects that fulfill also the condition  $z > 0.07$ . Surprisingly, there is yet – to our knowledge – no *direct* determination of the local QLF based on BQS objects alone. We have therefore computed a QLF from this sample with the same methods used for our own data, taking magnitudes, survey limits, and areas from SG83. We show the results of these computations as a cumulative distribution in Fig. 3. (Since all other literature data are available only in binned form, we have also binned the BQS LF in  $M_B$ , to achieve a more uniform presentation.) As mentioned above, Galactic extinction is neglected for these data; at any rate, the effect should be very small.

The space densities found from the HES data are much higher than those derived from the BQS, with the discrepancy increasing with luminosity. For the most luminous sources, we find that there are almost an order of magnitude more low-redshift quasars per unit volume than discovered by the BQS. Possible reasons for this discrepancy are discussed in Sect. 5.

#### 4.2. The space density of Seyfert 1 nuclei

To extend the local luminosity function towards fainter levels of nuclear activity, we have used the additional Seyfert 1 sample with  $z < 0.07$ . The absolute magnitudes were computed in the approximation of Euclidean static geometry and neglecting  $K$  corrections. To obtain reliable and unbiased estimates for the accessible volumes, the maximum redshift  $z_{\max,i}$  at which object  $i$  would still have been included in the survey had to be determined for each object. Because of the superposition of a host galaxy with constant intrinsic scale length and a point-like nucleus, the small-aperture magnitudes depended on redshift in a complicated way, and  $z_{\max,i}$  was therefore not only a function of  $B$  and  $B_{\text{lim}}$  but also of intrinsic properties. We used the available CCD images to simulate the mixing of AGN/host contributions into the aperture as a function of redshift  $z$ , resulting in an array of  $z_{\max,k}$  values, one for each field  $k$ . For simplicity, Table 3 supplies ‘effective’ values  $z_{\max}$  that permit a direct conversion into space densities. A  $V/V_{\max}$  test (Schmidt 1968), implemented in the generalisation proposed by Avni & Bahcall (1980), gives a mean value of  $V/V_{\max} = 0.43 \pm 0.11$  (individual values are also listed in Table 3). Compared with the expectation value of 0.5 for a complete, non-evolving, homogeneously distributed sample, there is no evidence for major incompleteness.

The resulting luminosity function is displayed in Fig. 4. It can be seen that a host galaxy correction is important particularly for the intrinsically faintest objects in the sample: Without correction, the luminosity function shows a steep upturn at  $M_B \simeq -20$ ; for these objects, even the small-aperture magnitude is dominated by the host rather than by the AGN.

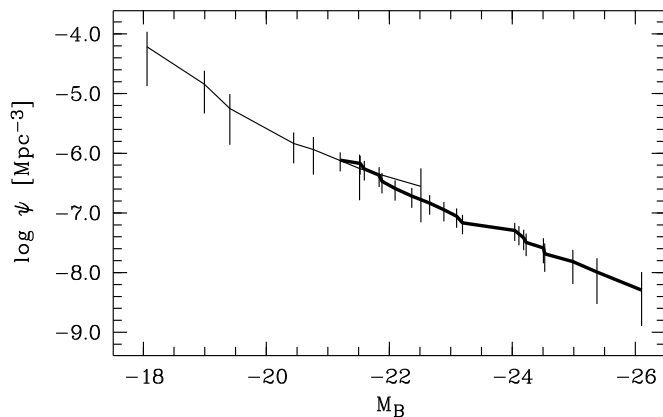


**Fig. 5.** Combined local luminosity function of quasars and Seyfert 1 nuclei with  $z < 0.3$ , based on magnitudes corrected for the host galaxies.

**Table 5.** Binned differential local luminosity function, computed from 27 QSOs and Seyferts with  $z < 0.3$ , in  $\text{Mpc}^{-3}$  per unit absolute magnitude interval centred on the value given by  $M_B$ . Column  $n$  gives the number of objects per bin.

$M_B$	$n$	$\phi(M_B)$	$\log \phi$
-18.5	2	$(5.5 \pm 4.7) \times 10^{-5}$	-4.3
-19.5	1	$(4.1 \pm 4.1) \times 10^{-6}$	-5.4
-20.5	2	$(9.0 \pm 6.7) \times 10^{-7}$	-6.0
-21.5	2	$(1.1 \pm 0.9) \times 10^{-7}$	-7.0
-22.5	8	$(4.5 \pm 1.8) \times 10^{-7}$	-6.4
-23.5	3	$(6.2 \pm 3.6) \times 10^{-8}$	-7.2
-24.5	6	$(3.6 \pm 1.5) \times 10^{-8}$	-7.5
-25.5	2	$(1.0 \pm 0.7) \times 10^{-8}$	-8.0
-26.5	1	$(5.0 \pm 5.0) \times 10^{-9}$	-8.3

Although the sample is not large, the derived space densities are fully consistent with previous estimates (Cheng et al. 1985; Huchra & Burg 1992). However, none of these previous investigations have paid as much attention to an appropriate host galaxy correction, neither for source luminosities nor for the survey volume, as we have. In particular, the analysis of the CfA sample by Huchra & Burg was based on uncorrected Zwicky magnitudes (essentially measuring the *total* galaxy brightness), making a straightforward comparison impossible. More similar to our approach was the work of Cheng et al. (1985) with Markarian galaxies, but their sample, although much larger than ours, had to be manipulated with substantial incompleteness corrections, in addition to the afore mentioned problems of a heterogeneous photometric data base.

#### 4.3. The combined local luminosity function

The local universe is the only domain where it is possible to construct the entire QLF, including low-luminosity tail, directly from one single survey. The local luminosity func-

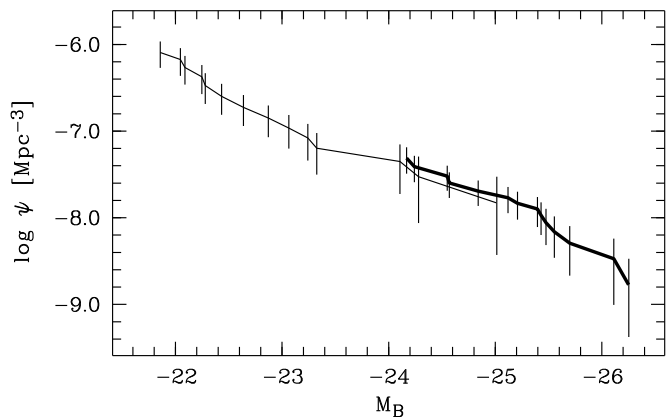


**Fig. 6.** The bright end of the quasar luminosity function up to  $z = 0.5$ , in comparison with the local QLF. Shown are the cumulative relations in the redshift shells  $z < 0.2$  (thin line), and  $0.2 < z < 0.5$  (thick line).

tion of QSOs and Seyfert 1 nuclei, obtained by combining the two independently derived luminosity functions presented above, is valid between absolute magnitudes  $-18$  and  $-26$ , thus spanning three decades in luminosity.

Overlaying the cumulative relations of Figs. 3 and 4, the match in the common luminosity region is remarkably good (cf. Fig. 5). To arrive at a consistent system of *nuclear* luminosities, the magnitudes in the QSO sample were corrected by subtracting a template host galaxy of  $M_B = -21$ . Since the magnitudes had already been measured through a small aperture, this host subtraction was a minor correction for all objects in the QSO sample, and the results are not sensitive to the assumed host luminosity.

The combined local QLF can be fitted well by a simple linear relation between  $M_B$  and  $\log \psi(M)$ , corresponding to a single power-law for the *differential* QLF ( $\phi(L)dL \propto L^\alpha$ ). A slope parameter  $\alpha = -2.17 \pm 0.06$  provides a statistically acceptable fit over the full range of 8 magnitudes. Fitting only the QSO sample ( $z > 0.07$ ) does not alter the slope significantly ( $\alpha = -2.10 \pm 0.08$ ); fitting only the  $z < 0.07$  Seyferts yields  $\alpha = -2.38 \pm 0.23$ , again consistent with a constant slope of  $\alpha \simeq -2.2$ . The slope of the BQS LF is much steeper: Apart from flattening at both high and low luminosities, the data demand  $\alpha \lesssim -3$  over the most of the range.

From the combined dataset, we have also produced a binned differential luminosity function  $\phi(M)$ , tabulated in steps of one in absolute magnitude (Table 5). As was to be expected, this representation is quite sensitive to the actual choice of binning intervals, most obvious in the succession of a ‘high’ and a ‘low’ bin at  $M_B = -22.5$  and  $-21.5$ , respectively. There is, however, full consistency of the results obtained; in particular, the QLF slope parameter  $\alpha \simeq 2.2$  is reproduced within the expected uncertainties.

#### 4.4. The quasar luminosity function at higher redshifts

The sample of Table 2 contains eight QSOs with redshifts  $0.3 < z < 0.5$  that we used to further constrain the potential error introduced by neglecting differential evolution. Binning the full  $z < 0.5$  sample into two redshift regimes  $0.07 < z < 0.2$  and  $z > 0.2$ , respectively, there are 14 objects in each shell. The luminosity functions are compared in Fig. 6: For  $-25 \lesssim M_B \lesssim -24$ , the local and the adjacent  $0.2 < z < 0.5$  shell have essentially identical space densities, while for  $M_B < -25$ , the QLF in  $z > 0.2$  seems to be merely a continuation of the local QLF to higher luminosities, *with the same slope and normalisation*. Dividing the sample at  $z = 0.3$  instead of 0.2 does not affect the results.

Outside the local universe, a single survey can yield no more than a small segment of the QLF, and only the combination of many different surveys can provide similar coverage of source luminosities as in the local QLF. The HES has the potential to provide new samples covering the brightest parts of the known QSO population, and it will be a promising task for the future to combine our results with those of fainter surveys. Such an analysis is, however, not the scope of the present paper. We only remark that even at redshifts higher than  $z = 0.5$ , the QLF pieces sampled by the HES do not show significant deviations from an extrapolation of the local relation. A more quantitative discussion of this issue is deferred to a later paper.

## 5. Discussion

### 5.1. Incompleteness of the BQS

Our results imply that the Palomar Bright Quasar Survey is not only incomplete, but also heavily biased. The general incompleteness may be estimated from the surface densities to be around a factor of 2–3. This effect has been noted by others before (Wampler & Ponz 1985; Goldschmidt et al. 1992), and we have at present no easy explanation for it. Some mild adjustment of the BQS data to higher values of space densities and luminosities may be required because of neglected Galactic extinction, but this cannot account for the observed discrepancy. One possibility is that the rather large photometric errors in the BQS, reflected in the  $(U - B)$  colours, scattered many QSOs out of the UV excess domain.

There seems to be an additional deficit of luminous low-redshift QSOs, by another factor of  $\gtrsim 2$  for  $M_B < -24$ . This discrepancy is apparent already from simply counting the number of  $z < 0.3$  QSOs more luminous than  $M_B = -24.5$ : There are 5 objects in the present HES sample, while the entire BQS contains only 15 such sources, in a more than 15 times larger area. As this is the first detection of such an effect, one has to carefully consider systematic errors. Note, however, that the HES is the first optical QSO survey since completion of the BQS that is

sensitive to a similar range of redshifts and luminosities, and it is therefore not altogether inconceivable that substantial selection biases have remained unnoticed over a long time.

The good agreement between the HES  $z > 0.2$  or  $z > 0.3$  surface densities with other major surveys, e.g., the LBQS (Hewett et al. 1995), the Edinburgh survey (Goldschmidt et al. 1992), or the HBQS (Cristiani et al. 1995), makes it implausible that the HES photometric zero-point could be seriously in error.

We also tested our method of zero-point corrected CCD photometry. All relevant quantities were recomputed based on the standard approach of using only photographic magnitudes measured over large apertures, without any systematic change of results, except that the luminosities of low-redshift QSOs with bright host galaxies were often *overestimated* in the photographic data, creating a bias towards even higher QLF values. The CCD approach thus seems justified and appropriate.

The reconstruction of the  $0.07 < z < 0.3$  luminosity function for the BQS was based on the same procedures as applied to our own data. We neglected differential evolution within the  $z < 0.3$  shell, but the *observed* discrepancy is independent of any assumed evolution law, and therefore most likely caused by real incompleteness in the BQS sample.

The exclusion of objects of non-stellar appearance in the BQS is an intuitively appealing candidate mechanism for this additional incompleteness. It is obvious at first glance (and has in fact never been disputed) that the BQS sample is systematically lacking low-luminosity Seyferts; it has usually been assumed that this selection effect ceased to be valid for  $M_B \lesssim -23$ . Our results suggest that this is not the case. However, it is then somewhat surprising that the incompleteness should be smallest, almost disappearing, in the luminosity range around  $M_B \simeq -23$ , as seems to follow from Fig. 3. In fact, this would then be the *only* region of the entire Hubble diagram where the BQS counts were not significantly below those of the HES.

Increased incompleteness for the most luminous QSOs seems a possible, but rather unlikely explanation. If, instead, the BQS magnitudes particularly for the slightly resolved  $M_B \simeq -23$  objects were *systematically too bright*, overcompleteness would occur, scattering objects into the sample from below the flux limit. We know from our own experience with photometry of resolved objects on digitised photographic plates that such effects exist, especially if a large digitisation aperture is used (this is why we decided to incorporate the CCD measurements). The BQS was based on PDS scans with an aperture of  $4''4$  (Green & Morril 1978), and magnitudes were basically isophotal in photographic density. We *suspect* that these technical details provide a clue to the above contradiction, and that incompleteness due to the rejection of extended QSO hosts could be partly counteracted by photometric bias



and overcompleteness for only marginally resolved objects. Further analysis of this point is certainly required.

If our hypothesis is correct, two important conjectures can be made: (1) The slope of the QLF for  $M_B < -23$  is much flatter than previous investigators estimated, weakening the evidence for a ‘break’ in the Seyfert/QSO transition regime (e.g., Marshall 1987) – the local QLF presented here showing essentially *no* break at all. Note that also in the Seyfert LF of Cheng et al. (1985), the presence of such a break is not really demanded by the data. (2) The BQS sample, up to now the prime source for luminous radio-quiet low-redshift QSOs, might suffer from severe selection biases with respect to the morphological properties of their galaxy hosts.

### 5.2. Constraints on quasar evolution

The local luminosity function derived in this paper is independent of samples collected at higher redshifts, and therefore well suited to test and constrain possible evolution laws. Existing estimates of the QLF at redshift  $z \simeq 2$  (e.g., Boyle et al. 1991) show a marked break, or change of slope, at intermediate luminosities, that shifts towards lower values with decreasing  $z$ . We have argued above that the local equivalent of this break is probably an artefact. The flat slope of the  $z \approx 0$  QLF derived in this paper, and the absence of clear features, demand, on the assumption that the high  $z$  QLF determinations are correct, that both shape and slope of the QLF change strongly with redshift. This clearly is in contradiction to the ‘standard picture’ of pure luminosity evolution (PLE), where a double power-law luminosity function with invariant logarithmic shape is merely shifted along the luminosity axis.

However, it should be noted that virtually *all* evolution modelling since 1983 had to rely on the BQS data of SG83, to cover an otherwise inaccessible part of the Hubble diagram. Hence, in these regions, the models merely reproduce the incompleteness and possible biases of the BQS contribution. The problem that QSO surveys were notoriously incomplete at low redshifts was of course realised by most researchers, and it has become customary to apply a lower redshift cutoff of  $z_{\min} \simeq 0.3$  to all samples. The construction of a  $z = 0$  QLF from such models has therefore always the character of an *extrapolation* outside the validated range, and should be treated with appropriate caution. Even so, a *quantitative* comparison between evolutionary models and actual measurements of the local Seyfert 1/QLF is a powerful test which deserves higher attention than it has been paid to in the past, compared to the careful analyses of higher redshift data.

In the construction of the  $z < 0.3$  local QLF we have not corrected individual luminosities for statistical evolution. While it is true that such a neglect could artificially flatten the luminosity function, evolution must be fairly strong for the effect to be relevant. We show now that the no-evolution assumption was, in fact, the best approxi-

mation one could possibly make, over the range of luminosities covered by the HES. In the case of evolution, the LFs of adjacent, non-overlapping redshift shells should be different. For the simple case of PLE with the rate suggested, e.g., by Boyle et al. (1991), one would expect an abscissa offset of  $\Delta M = -0.8$  mag between  $z < 0.2$  and  $0.2 < z < 0.5$ . The necessity to invoke such an offset is not apparent from Fig. 6. While it might be consistent with our data to allow for a somewhat steeper intrinsic slope of the QLF, combined with mild evolution, there is certainly *no evidence* for evolution in the data.

These conclusions are supported by results reported recently from other surveys. Hewett et al. (1993), with a preliminary analysis of the LBQS, showed that the QLF flattens considerably at  $z < 1$ ; a similar conclusion was reached by Miller et al. (1993) using the Edinburgh survey. Although both surveys have the usual lower redshift limit excluding the local population ( $z > 0.3$  for the Edinburgh survey,  $z > 0.2$  for the LBQS), a prediction for the slope of the local QLF can be made by extrapolating the trend seen by Miller et al.; the result is consistent with our measured value of  $\alpha = -2.2$ . A flatter QLF implies a higher fraction of luminous quasars among the total population. Our results indicate therefore, in agreement with Hewett et al. and Miller et al., that the evolution of the most luminous quasars must proceed considerably slower than suggested by the notion of pure luminosity evolution.

## 6. Conclusions and outlook

We have analysed a new, flux-limited and well-defined sample of QSOs & Seyfert 1 galaxies. Host-galaxy dependent selection and photometric biases, if not absent, are greatly reduced in comparison to other optically selected samples. We find that the derived space density of luminous QSOs in the local universe is much higher than previous surveys indicated, and that consequently these objects show a much slower cosmological evolution.

With the present sample of 55 QSOs and Seyferts in 33 fields, only a small fraction of the HES area is covered. We have already acquired, and partly processed, much additional plate material enlarging the survey by a significant factor. For example, we now have several fields in common with the BQS, and it shall soon be possible to pursue the question of incompleteness and biases in the BQS by a direct comparison of objects and photometry.

To understand and model the process of quasar evolution requires strong constraints from observations. It seems now that we are farther away from a coherent empirical picture of the QSO population and its evolution than thought a few years ago. Quasars of different luminosities evolve differently, and quasars do not necessarily evolve with the same rate at different cosmological epochs. There are presumably more parameters needed to describe quasar evolution properly than in the simple model of ‘pure luminosity evolution’.

The ultimate aim of QSO survey work is the deduction of intrinsic physical properties from statistical samples. Unfortunately the physical processes in active galaxy nuclei are poorly understood, and the relations between statistical and physical properties therefore far from unique. The best study cases for nuclear activity in galaxies are nearby Seyferts; as shown above, the luminosity function of Seyfert 1 nuclei can be smoothly continued into the classical quasar regime, without a significant change of slope or break. While this by no means proves that Seyfert 1 nuclei are simply scaled-down versions of quasars, it suggests a continuity of properties rather than distinct classes. With the completion of the HES, a large and well-defined sample of highly luminous low-redshift QSOs will become available, to study the relationship between QSOs, their environments, and their evolution in detail.

This article was processed by the author using Springer-Verlag L<sup>A</sup>T<sub>E</sub>X A&A style file *L-AA* version 3.

*Acknowledgements.* T.K. acknowledges support from the Deutsche Forschungsgemeinschaft under grant Re 353/33. Substantial observing time at ESO was allotted to the project as ESO key programme 02-009-45K.

## References

- Avni Y., Bahcall J.N., 1980, ApJ 235, 694  
 Boyle B.J., Jones L.R., Shanks T., 1991, MNRAS 251, 482  
 Cheng F.-z., Danese L., De Zotti G., Franceschini A., 1985, MNRAS 212, 857  
 Cristiani S., Vio R., 1990, A&A 227, 385  
 Cristiani S., La Franca F., Andreani P., et al., 1995, A&AS 112, 347  
 Felten J.E., 1976, ApJ 207, 700  
 Goldschmidt P., Miller L., La Franca F., Cristiani S., 1992, MNRAS 256, 65  
 Green R.F., Morrill M.E., 1978, PASP 90, 601  
 Hewett P.C., Foltz C.B., Chaffee F.H., 1993, ApJ 406, L43  
 Hewett P.C., Foltz C.B., Chaffee F.H., 1995, AJ 109, 1498  
 Huchra J., Burg R., 1992, ApJ 393, 90  
 Köhler T., 1996, Doctoral Thesis, Universität Hamburg  
 Marshall H., 1987, AJ 94, 628  
 Miller L., Goldschmidt P., La Franca F., Cristiani S., 1993, Observational Cosmology, eds. G. Chincarini et al., ASP Conf. Proc. 51, 614  
 Reimers D., Köhler T., Wisotzki L., 1996, A&AS 115, 235 (Paper II)  
 Sandage A., 1973, ApJ 180, 687  
 Schmidt M., 1968, ApJ 151, 393  
 Schmidt M., Green R.F., 1983, ApJ 269, 352 (SG83)  
 Spitzer L., 1978, Physical Processes in the Interstellar Medium, Wiley&Sons  
 Stark A.A., Gammie C.F., Wilson R.W., et al., 1992, ApJS 79, 77  
 Terrell J., 1977, Am. J. Phys. 45, 869  
 Véron-Cetty M.-P., Véron P., 1993, A Catalogue of Quasars and Active Galactic Nuclei, 6th ed., ESO Scientific Report 13  
 Wampler E.J., Ponz D., 1985, ApJ 298, 448  
 Wisotzki L., Köhler T., Groote D., Reimers D., 1996, A&AS 115, 227 (Paper I)